Electrostatics in disordered Cu_xPd_{1-x} alloys

1998 J. Phys.: Condens. Matter 10 5679

(http://iopscience.iop.org/0953-8984/10/25/017)

J. Phys.: Condens. Matter **10** (1998) 5679–5695. Printed in the UK PII: S0953-8984(98)91735-0

Electrostatics in disordered Cu_xPd_{1-x} alloys

R J Cole and P Weightman

Surface Science Research Centre, University of Liverpool, Liverpool L69 3BX, UK

Received 17 February 1998

Abstract. The distribution of site potentials in random substitutionally disordered alloys is investigated. Within the correlated charge model (CCM), where the charge on a site is proportional to its number of 'unlike' nearest neighbours, the site potential is found to be determined predominantly by the composition of the first shell. It is shown that the distribution of site potentials implicit in the CCM implies a modest but measurable 'disorder' broadening of the core level XPS spectra of disordered alloys. Experimental results demonstrating this effect for the Cu_xPd_{1-x} alloy system are presented.

1. Introduction

In recent years the inclusion of Madelung energies for disordered systems, often implicitly assumed to be zero, has been shown to be essential to a truly *ab initio* description of the physical and electronic structure of random alloys [1], stimulating considerable interest in the Madelung problem and the determination of local charges in these systems. The 'correlated charge model', in which the charge on a site is determined by the local composition, has gained increasing support [1, 2], and has been used to explain the structural stability of a wide range of compounds and alloys [3].

Core level x-ray photoelectron spectroscopy (XPS) provides a measure of the potential at the lattice sites of solids. One expects that variation in local bonding configuration in disordered systems will give rise to a distribution of potentials and a 'disorder broadening' of core XPS spectra, in addition to a composition dependent average site potential shift. However, while chemical shifts in the core level binding energies of alloys are routinely observed, the first experimental evidence for disorder broadening of core level photoelectron lines has only very recently been presented [4]. In the present work we consider the effects of disorder on the electrostatic potential in random substitutional Cu_xPd_{1-x} alloys.

The paper is organized as follows. In section 2 we discuss the distribution of site potentials in random systems and characterize this distribution on the basis of the correlated charge model [2]. The validity of the model is relevant to theoretical schemes for improving *ab initio* calculations of the total energies of disordered systems. The disorder broadening of core level XPS lines is discussed in section 3. Experimental data for the Cu_xPd_{1-x} alloy system is presented in section 4 and analysed in section 5. A discussion of the results and conclusions are presented in sections 6 and 7 respectively. This comparison of theoretical models and experimental results gives insight into local charge neutrality, short range order and charge correlation in disordered alloys.

0953-8984/98/255679+17$19.50

2. Potentials and core level binding energies

The electrostatic potential at lattice point i in a random alloy relative to the corresponding elemental solid can be expressed as a sum of intra-atomic and extra-atomic terms

$$V^i = \frac{14.4}{R}\left\{2Q^i + \sum_{m=1}^{\infty}\frac{1}{\rho_m}\sum_{j\in m}Q^j\right\}. \tag{1}$$

If the charges Q^i are measured in units of e (where the charge on the electron is $-1e$) and the nearest neighbour distance R is in angströms, then the potential is in volts (we supress the 14.4 factor in subsequent potential equations for brevity.) The first summation in the extra-atomic term (usually referred to as the Madelung potential) is over concentric shells with radius $R\rho_m$ centred on site i, while the second is over the Z_m sites in the mth shell.

We consider an unspecified Bravais lattice which we populate with A and B atoms, asigning an occupation variable S^i to each site such that $S^i = -1(+1)$ if i is occupied by an A(B) atom. To characterize the distribution of potentials in the random alloy we require a model for the charge at each site. Chemical wisdom suggests that an atom surrounded by all 'like' atoms will be approximately neutral while an atom surrounded by all 'unlike' atoms will experience the maximum possible charge transfer. This means that the *charges* Q^i in a random system are correlated even when the *site occupations* S^i are truly random [2]. Magri *et al* have suggested [2] a correlated charge model (CCM) with the form

$$Q^i = \lambda\sum_{j\in 1}(S^i - S^j) = 2\lambda N_1 S^i \tag{2}$$

where N_1 is the number of unlike neighbours in the first shell, λ determines the ionicity, and $j \in 1$ denotes the set of sites in the first shell of site i. It has been shown [3] that this model predicts the structural stability of a wide range of compounds and alloys. We now investigate the distribution of potentials in the random CCM lattice.

2.1. The distribution of potentials

We consider first the dependence of the lattice site potential on N_1, averaging over all possible compositions and configurations of all subsequent shells. Averaging over those A(B) sites that have N_1 unlike nearest neighbours, equation (1) becomes

$$\langle V(N_1)\rangle_{\mathrm{A(B)}} = \frac{1}{R}\sum_{m=0}^{\infty}\frac{\langle Q_m(N_1)\rangle_{\mathrm{A(B)}}}{\rho_m} \tag{3}$$

where

$$Q_m = \sum_{j\in m}Q^j \tag{4}$$

is the charge on the mth shell. For compactness we have absorbed the intra-atomic term into the shell sum. The charge on the 'zeroth' shell Q_0, is simply the charge on the central site, and we assume $\rho_0 = 1/2$. Using equation (2) we obtain [4, 5]

$$\langle Q_1(N_1)\rangle_{\mathrm{A(B)}} = -2\lambda S^{\mathrm{A(B)}}Z_1\left(1-c^{\mathrm{A(B)}}\right) - 2\lambda S^{\mathrm{A(B)}}\left\{Z_1\left(1-c^{\mathrm{A(B)}}\right) - N_1\right\}\left(K_1^1 - Z_1\right) \tag{5}$$

where K_m^1 is the number of sites that are simultaneously in the first shell of the central site and nearest neighbours of a site in the mth shell [1]. The choice of the central site and its nearest neighbour composition does not impose any selection criteria on the site occupations of any subsequent shells, but the charge on any shell containing sites which share nearest

neighbours with the central site (i.e. $K_m^1 \neq 0$) will be indirectly influenced. For these shells we find

$$\langle Q_{m>1}(N_1)\rangle_{\mathrm{A(B)}} = -2\lambda S^{\mathrm{A(B)}} K_m^1 \left\{ Z_1 \left(1 - c^{\mathrm{A(B)}}\right) - N_1 \right\}. \tag{6}$$

Equation (3) can now be rewritten:

$$\langle V(N_1)\rangle_{\mathrm{A(B)}} = 2\frac{\lambda}{R} S^{\mathrm{A(B)}} Z_1 \left(1 - c^{\mathrm{A(B)}}\right) + 2\frac{\lambda}{R} S^{\mathrm{A(B)}} \left\{ Z_1 \left(1 - c^{\mathrm{A(B)}}\right) - N_1 \right\} (Z_1 - \Sigma_1) \tag{7}$$

where Σ_1 is the lattice dependent constant defined by

$$\Sigma_1 = \sum_{m=0}^{\infty} \frac{K_m^1 Z_m}{\rho_m Z_1}. \tag{8}$$

Values of K_m^1, Z_m and ρ_m can be found in table 1 for the fcc lattice. It is clear from equation (7) that $\langle V(N_1)\rangle_{\mathrm{A(B)}}$ is linear in N_1 with gradient independent of composition. The Madelung part of $\langle V(N_1)\rangle_{\mathrm{A(B)}}$ scales faster with N_1 than the intra-atomic part but with opposite sign to $S^{\mathrm{A(B)}}$, and so the total potential varies with $-N_1 S^{\mathrm{A(B)}}$ [5]. For the CuPd alloy system Lu *et al* [6] have obtained $\lambda = 5.5 \times 10^{-3} e$ from first principles calculations for ordered CuPd structures. Combining this value with the Cu lattice parameter we obtain $\lambda/R \sim 2.2 \times 10^{-3} e$ Å^{-1}. For the fcc lattice with this value of λ/R the gradient of $\langle V(N_1)\rangle$ against N_1 is 0.11 V, implying a measureable disorder broadening of alloy core level XPS spectra [7].

Table 1. Structural parameters for the fcc lattice.

m	Z_m	ρ_m	Σ_m	K_0^m	K_1^m	K_2^m	K_3^m	K_4^m	K_5^m
0	1	1/2	24	0	1	0	0	0	0
1	12	1	10.22	12	4	4	2	1	0
2	6	$\sqrt{2}$	8.10	0	2	0	1	1	1
3	24	$\sqrt{3}$	6.92	0	4	4	2	4	2
4	12	2	6.05	0	1	0	2	0	1
5	24	$\sqrt{5}$	5.35	0	0	4	2	2	2

We now consider the variation in site potential caused by variations in the composition of more distant shells. If the composition of the first ℓ shells is denoted $N_1, N_2, \cdots, N_\ell$, where N_m is the number of unlike neighbours in the mth shell, it can be shown that the charge on the mth shell where $m \leqslant \ell$ is given by

$$\begin{aligned}\langle Q_m(N_1, N_2, \cdots, N_\ell)\rangle_{\mathrm{A(B)}} &= 2Z_1 S^{\mathrm{A(B)}} \lambda \left\{ Z_m \left(1 - c^{\mathrm{A(B)}}\right) - N_m \right\} \\ &\quad -2S^{\mathrm{A(B)}} \lambda \sum_{\alpha=0}^{\ell} K_\alpha^m \left\{ Z_\alpha \left(1 - c^{\mathrm{A(B)}}\right) - N_\alpha \right\}\end{aligned} \tag{9}$$

while for $m > \ell$ we obtain

$$\langle Q_m(N_1, N_2, \cdots, N_\ell)\rangle_{\mathrm{A(B)}} = -2S^{\mathrm{A(B)}} \lambda \sum_{\alpha=0}^{\ell} K_\alpha^m \left\{ Z_\alpha \left(1 - c^{\mathrm{A(B)}}\right) - N_\alpha \right\}. \tag{10}$$

In deriving equations (9) and (10) the relation $Z_m K_m^\alpha = K_\alpha^m Z_\alpha$ has been used, where K_α^m is the number of sites that are simultaneously in the mth shell aound the central site and nearest neighbours of a site in the αth shell. The leading elements of the K matrix for the

fcc lattice are given in table 1. The average potential for A(B) sites with the compositions of the first ℓ shells constrained can now be written

$$\langle V(N_1, N_2, \cdots, N_\ell)\rangle_{\mathrm{A(B)}} = \frac{2\lambda}{R} S^{\mathrm{A(B)}} \sum_{\alpha=0}^{\ell} \left\{ Z_\alpha \left(1 - c^{\mathrm{A(B)}}\right) - N_\alpha \right\} \left\{ \frac{Z_1}{\rho_\alpha} - \Sigma_\alpha \right\} \tag{11}$$

where

$$\Sigma_\alpha = \sum_{m=0}^{\infty} \frac{K_m^\alpha Z_m}{\rho_m Z_\alpha} = \sum_{m=0}^{\infty} \frac{K_\alpha^m}{\rho_m}. \tag{12}$$

The effect of disorder in the composition of the ℓth shell on the site potentials can be evaluated as the difference between $\langle V(N_1, N_2, \cdots, N_{\ell-1})\rangle_{\mathrm{A(B)}}$ (where we have averaged over N_ℓ) and $\langle V(N_1, N_2, \cdots, N_{\ell-1}, N_\ell)\rangle_{\mathrm{A(B)}}$ (where N_ℓ is now specified). It is straightforward to show that

$$\begin{aligned}\langle V(N_1, N_2, \cdots, N_{\ell-1}, N_\ell)\rangle_{\mathrm{A(B)}} - \langle V(N_1, N_2, \cdots, N_{\ell-1})\rangle_{\mathrm{A(B)}} \\ = 2\frac{\lambda}{R} S^{\mathrm{A(B)}} \left\{ Z_\ell \left(1 - c^{\mathrm{A(B)}}\right) - N_\ell \right\} \left\{ \frac{Z_1}{\rho_\ell} - \Sigma_\ell \right\}.\end{aligned} \tag{13}$$

For each shell the probability for a given value of N_m is given by

$$P_m^{\mathrm{A(B)}}(N_m, c^{\mathrm{A(B)}}) = \frac{Z_m! \left(c^{\mathrm{A(B)}}\right)^{Z_m - N_m} \left(1 - c^{\mathrm{A(B)}}\right)^{N_m}}{(Z_m - N_m)! N_m!}. \tag{14}$$

The maximum width of $P_m(N_m, c^{\mathrm{A(B)}})$ against N_m (and so the greatest core XPS broadening effect) is attained when $c^{\mathrm{A}} = c^{\mathrm{B}} = 0.5$. At this composition the probability envelope for each shell is approximately Gaussian and we expect a Gaussian broadening of the core XPS spectrum. For other compositions the function $P_m(N_m, c^{\mathrm{A(B)}})$ is asymmetric and narrows since less disorder is possible; in a sense there is no disorder at the impurity limit. For a given composition, the probability distribution given by equation (14) has the same general shape for all shells. It follows that the effect of compositional disorder in increasingly distant shells is to introduce increasingly fine but 'self-similar' structure into the distribution of potentials at the central site. The scale of this fine structure is given by the factor $\{(Z_1/\rho_\ell) - \Sigma_\ell\}$ in equation (13). For the fcc lattice this quantity is rapidly convergent and most of the disorder in the potentials is due to disorder in the composition of the first shell. This is illustrated in figure 1 where the effects on the average A site potentials of compositional disorder in the first three shells of the fcc lattice is shown for $c^{\mathrm{A}} = 0.5$ and $c^{\mathrm{A}} = 0.8$.

In a previous study [5] the site potentials were calculated for large clusters with the charges on each site determined by the CCM. Cluster results showing the distribution of potentials for each value of N_1 are shown in figure 2 for $c^A = 0.5$ and 0.8. The results of these cluster calculations clearly demonstrate that the potential at a site is determined predominantly by the composition of its nearest neighbour shell, confirming the analytical results of figure 1. For $c^A = 0.8$ the self similarity of the distributions derived from the first and second shells can also be seen.

2.2. Chemical shifts

We consider briefly the core level binding energy shifts predicted by the CCM. For an ordered system a chemical shift in core level photoelectron binding energy relative to the corresponding elemental solid can be expressed in the form [8]

$$\Delta E_b^{\mathrm{A(B)}} \approx e\Delta V^{\mathrm{A(B)}} = e\Delta Q^{\mathrm{A(B)}} \left(\frac{2}{R} - \frac{\alpha}{R} \right) \tag{15}$$

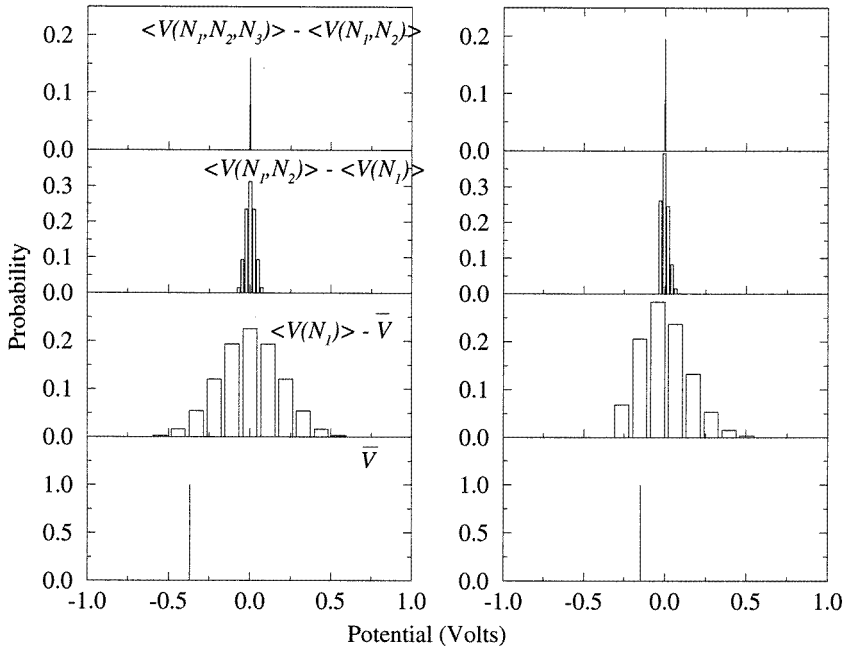

Figure 1. The effect of compositional disorder in increasingly distant shells on the average potential at A sites in fcc alloys. The left and right panels correspond to $c^{\mathrm{A}} = 0.5$ and $c^{\mathrm{A}} = 0.8$ respectively. In each case the bottom panel indicates $\overline{V}$, the average A site potential. The next panel gives the distribution of potentials due to each possible value of N_1 (i.e. compositional disorder in the first shell) The third and fourth panels indicate the broadening due to compositional disorder in the second and third shells respectively. In the histogram for each shell the values of N_m increase from left to right from 0 to $Z_m 0$.

where α is the Madelung constant and the approximation in the first equality is due to the neglect of relaxation energy shifts. For a random alloy within the CCM the average A site charge $\overline{Q}^{\mathrm{A}}$ is given by

$$\overline{Q}^{\mathrm{A}} = 2\lambda S^{\mathrm{A}} Z_1 \left(1 - c^{\mathrm{A}}\right). \tag{16}$$

It has been shown [5] that there is on average a charge of $-\overline{Q}^{\mathrm{A}}$ in the first shell, while all subsequent shells are on average charge neutral, implying perfect screening (on average) within the nearest neighbour shell. Shells with $m > 1$, $K_m^1 \neq 0$ contribute to the average Madelung energy but do not contribute to the average potential $\overline{V}$. Clearly for disordered systems a distinction must be made between Madelung constants corresponding to the electrostatic *potential* and the electrostatic *energy*. For the CCM Magri *et al* [2] have shown that the energy constant exhibits a parabolic variation with composition. The average site potential is

$$\overline{V}^{\mathrm{A(B)}} = 2\frac{\lambda}{R} S^{\mathrm{A(B)}} Z_1 \left(1 - c^{\mathrm{A(B)}}\right) = \frac{\overline{Q}^{\mathrm{A(B)}}}{R} \tag{17}$$

and so by analogy with equation (15) the effective Madelung (potential) constant for disordered alloys within the CCM is $\alpha^{eff} = 1$ for all lattices and for all compositions. This result may be contrasted with that for standard 'single site' models where all A(B) sites are considered to be equivalent. In the single site approach the charges $Q^{\mathrm{A(B)}}$ do not

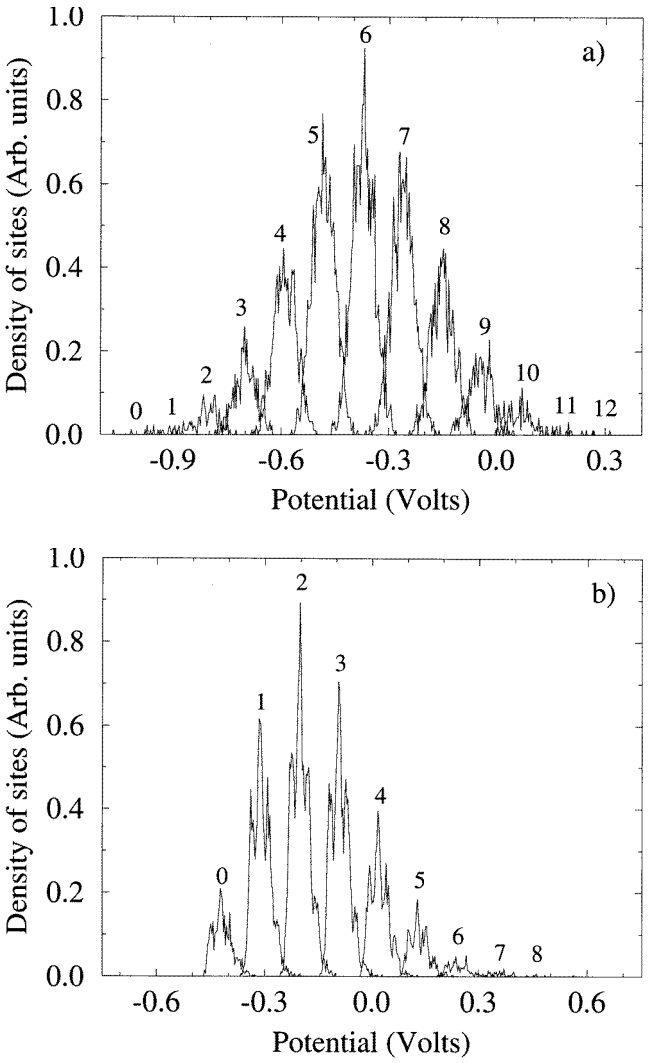

Figure 2. Density of A sites with a given value of V^i for fcc clusters with composition $c^{\mathrm{A}} = 0.5$ (a) and $c^{\mathrm{A}} = 0.8$ (b) In each case separate curves are plotted for each possible value of N_1.

vary with local coordination, but instead are determined by the global composition and the constraint of charge neutrality. Madelung effects must then vanish on average (i.e. $\alpha^{eff} = 0$) and there is on average no screening at all.

3. Core level XPS spectra

Having determined the effects of disorder on the site potentials in a substitutionally disordered alloy we now go on to consider the resulting core level XPS spectra. We can use the potentials calculated for large clusters to simulate XPS spectra using the expression

$$\langle f^i(\omega)\rangle_{\mathrm{A(B)}} = \frac{1}{n^{\mathrm{A(B)}}} \sum_{i=\mathrm{A(B)}} L^{\Gamma}(\omega, V^i) \tag{18}$$

where $n^{A(B)}$ is the number of A(B) sites in the cluster and we have assumed that the component spectra $f^i(\omega)$ are given by $L^\Gamma(\omega, V^i)$, Lorentzians with FWHM Γ and position determined by the site potentials V^i. The more compact expression

$$\langle f^i(\omega)\rangle_{A(B)} \approx \sum_{N_1=0}^{Z_1} P(N_1) L^\Gamma(\omega, \langle V(N_1)\rangle_{A(B)}) \tag{19}$$

is suggested by the demonstration in section 2 that the V^i are determined primarily by the composition of the nearest neighbour shell. We refer to this expression as the 'nearest neighbour approximation' (NNA). A further approximation

$$\langle f^i(\omega)\rangle_{A(B)} \approx L^\Gamma(\omega, \overline{V}^{A(B)}) \tag{20}$$

referred to as the 'average neighbour approximation' (ANA) assumes a single effective A(B) environment which experiences the average potential $\overline{V}$. Comparison of $\langle f^i(\omega)\rangle$ determined using equations (18) (exact) and (20) (ANA) will determine explicitly the extent of disorder broadening. Comparison of equations (18), (19) and (20) is made for fcc clusters with $c^{A(B)} = 0.5$ and $c^{A(B)} = 0.8$ in figures 3(a) and (b) respectively. In each case Γ= 0.6 eV and a Gaussian broadening of W = 0.3 eV FWHM were used to simulate the Cu 2p lifetime broadening and experimental resolution respectively. λ/R was taken to be $2.2 \times 10^{-3} e$ Å^{-1}. For the parameters used disorder can be seen to significantly broaden the core spectrum. We find that the 13-component envelope generated by the NNA performs extremely well for all compositions.

The predicted Cu 2p core level binding energy shifts [9] for Cu_xPd_{1-x} alloys are plotted in figure 4 and are found [10] to be a good represention the experimental shifts [11, 12]. The predicted composition dependence of the core XPS FWHM is also shown in figure 4. For $c^{A(B)} = 0.5$ disorder in the site potentials leads to a predicted increase in FWHM of 0.23 eV. For $c^{A(B)} = 0.8$ the increase in FWHM is 0.16 eV, approximately 70% of the maximum value. Core level XPS spectra of disordered alloys have usually been measured with monochromated Al $K\alpha$ radiation with an experimental resolution of about 0.5 eV. The results in figure 3 show that 'third generation' XPS spectrometers, which achieve an experimental resolution of about 0.25 eV with a high photon flux, should be capable of observing disorder broadening of XPS lines in alloys with narrow core levels. The dominant contribution to the resolution of such spectrometers is usually the width of the excitation source. For elements with narrow *and shallow* core levels (e.g. the 4f levels of the metals Ta to Pb) soft x-ray excitation provided by low energy (<100 eV) synchrotron beamlines, where photon widths of 25 meV are now routinely achieved, should more readily reveal core level disorder effects. The first experimental results demonstrating a broadening of core XPS spectra have recently been presented [4]. The present work extends this earlier study.

A comparison of calculated site potentials for the surface (sites with missing nearest neighbours), subsurface (fully coordinated sites within a bond length from the surface), and bulk sites of substitutionally disordered CCM clusters has recently been made [5]. It was found that the subsurface is essentially bulk-like both in terms of its average site potentials $\langle V(N_1)\rangle$ and the distributions about these averages. The surface site potentials were found to have a slightly shallower dependence on N_1. These observations imply that the core XPS spectra of the CCM cluster can be simulated by the superposition of a bulk and a surface contribution, as is standard practice for elemental solids. XPS simulations including surface effects have also been performed [5], assuming a surface intensity 15% that of the

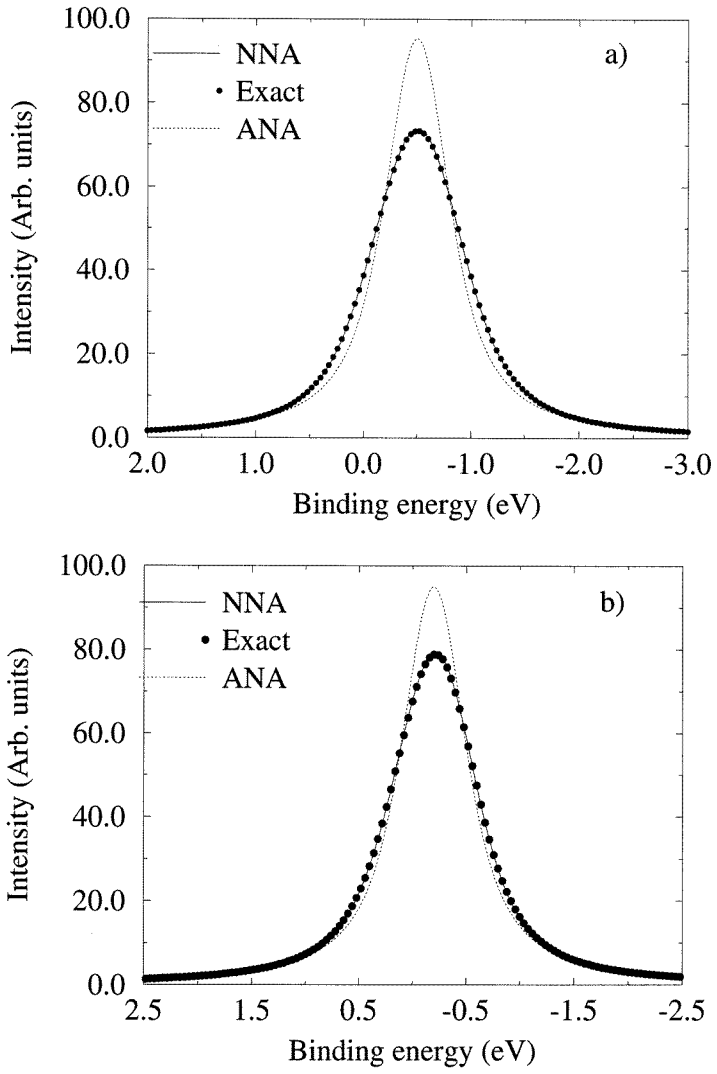

Figure 3. XPS simulations for fcc clusters with composition $c^{A} = 0.5$ (a) and $c^{A} = 0.8$ (b).

bulk signal and two important results were obtained. Firstly it was shown that the core level XPS lineshape is insensitive to the surface disorder broadening. Secondly it was found that the effect of bulk disorder broadening could not be reproduced by varying the energy of the surface component. Together these results suggest that when electron escape depths are large and so surface sensitivity is low (as is the case for the Cu 2p line excited by Al $K\alpha$ x-rays) one does not expect surface effects to present a fundamental barrier to the unambiguous experimental observation of bulk disorder broadening of core level XPS spectra.

Having characterized the disorder broadening of core XPS lines on the basis of the correlated charge model we now describe experimental results for the Cu_xPd_{1-x} alloy system.

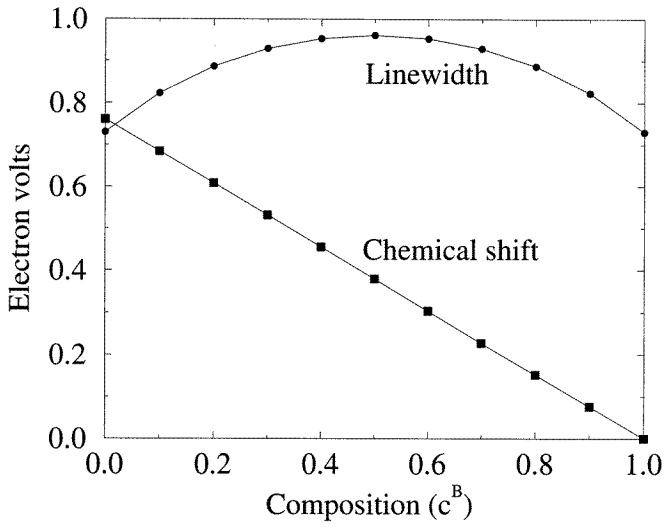

Figure 4. Calculated chemical shifts and linewidths for B sites as functions of composition in random fcc alloys. A value of $\lambda/R = 2.2 \times 10^{-3}$ has been used as discussed in the text.

4. Experimental results

Disordered polycrystalline samples of $Cu_{0.5}Pd_{0.5}$ and $Cu_{0.8}Pd_{0.2}$ were prepared by melting the required proportions of high purity component metals under Ar in an arc furnace followed by rapid quenching. Homogeneity was ensured by repeated remelting. Specimens were examined using the Scienta ESCA 300 spectrometer at the RUSTI facility at Daresbury Laboratory along with a pure Cu specimen. The specimen surfaces were mechanically cleaned *in situ* and photoelectron spectra were obtained at near normal emission using a monchromated Al anode x-ray source. Surface cleanliness was verified by the absence of C and O photoelectron signals.

Experimental Cu $2p_{3/2}$ photoelectron spectra are shown in figure 5(a) for Cu, $Cu_{0.5}Pd_{0.5}$ and $Cu_{0.8}Pd_{0.2}$. The photoelectron peaks of each sample have been aligned in energy and placed on the same ordinate scale by normalizing the intensities at the centre of the peak and at 20 eV higher kinetic energy. It can be seen that the intensity of the inelastic background in the region of the photoelectron peak is extremely low in all cases. It is also apparent from the raw data that the alloy spectra are broader than that of pure Cu. This broadening can be clearly observed on both sides of the peak but is more pronounced to lower kinetic energy.

It is instructive to normalize the experimental spectra according to total integrated intensity, as shown in figure 5(b). This representation of the raw data disguises the differences in linewidth of the main photoelectron line observed for the three specimens but demonstrates that the background contributions to the spectra are of equal intensity. The two alloy spectra are virtually indistinguishable on the high kinetic energy side of the peak but there is an increase in intensity in the low kinetic energy tail which increases with Pd concentration.

To summarize, two primary observations can be made from the raw data; namely that with increasing Pd concentration there is an increase in Cu 2p linewidth and an increase in

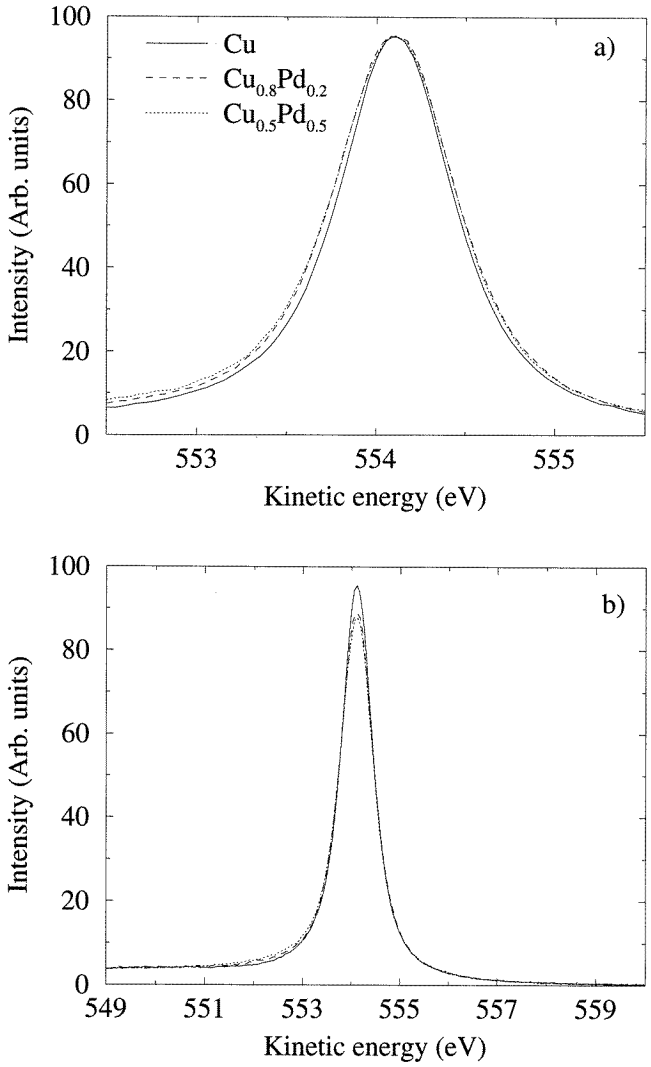

Figure 5. Experimental Cu $2p_{3/2}$ photoelectron spectra for Cu (solid curve), $Cu_{0.8}Pd_{0.2}$ (dashed curve), and $Cu_{0.5}Pd_{0.5}$ (dotted curve) The spectra have been normalized according to peak height in (a) and according to total intensity in (b). In each case the photoelectron peaks have been aligned in kinetic energy.

intensity in the low kinetic energy photoelectron tail. We now perform a detailed numerical analysis to provide quantification and enable interpretation of these effects.

5. Analysis

The most established method of analysing core level XPS spectra remains the least squares (LS) fitting of raw experimental data with a parameterized function [13], and this approach is used here. Fit quality is assessed by consideration of the residuals r_i given by $y_i - y_0(x_i)$, where (x_i, y_i) is the set of experimental data points, and $(x_i, y_0(x_i))$ is the set of simulated

data points [13, 14]. If the assumed form of the spectrum is a good representation of the experimental data, then the residuals after LS optimization should consist of random fluctuations due to statistical noise. Systematic variations in the residuals indicate the inadequacy of the functional form chosen for y_0. We will also quote for each fit the index χ_r^2 referred to as 'chi-squared per degree of freedom' and defined by

$$\chi_r^2 = \frac{1}{n_d - n_p} \sum_{i=1}^{n_d} \frac{(y_i - y_0(x_i))^2}{y_i} \tag{21}$$

where n_d is the number of experimental data points and n_p is the number of free parameters in the fitting function.

5.1. Cu

Although the XPS spectra of elemental metals contain distinct contributions from bulk and surface sites, the large escape depth for Cu 2p photoelectrons excited by Al $K\alpha$ radiation ensures low surface sensitivity. Surface core level emission from Cu has however been identified by Citrin, Wertheim and Baer (CWB) [14] by measuring the 2p spectrum as a function of emission angle relative to the surface normal, thereby enhancing surface sensitivity. Simultaneous analysis of such a series of spectra in terms of a bulk and a surface component enabled accurate determination of the surface core level shift.

We first attempted to fit our experimental Cu spectrum to a single Doniach–Šunjić (DS) lineshape [15] which is characterized by an inverse lifetime Γ and an asymmetry index α which parameterizes the many-body response of the electron gas to the sudden creation of a core hole potential. A Gaussian broadening W to simulate instrumental and phonon broadening was also included. A poor fit was obtained (see 'FIT 1' in table 2) and we observed the same systematics in the residuals, as found previously by CWB. Introducing a second component with position and intensity unconstrained (FIT 2 in table 2) we obtained $\chi_r^2 = 0.86$. The surface core level binding energy shift E_b^s and surface to bulk intensity ratio I^s were found to be -0.27 ± 0.03 eV and 0.14 ± 0.06 respectively, in good agreement with CWB. Although an independent fit provided a worthwhile check on the consistency of the present work with CWB, we consider the core level shift determination of CWB to be more accurate due to their surface sensitive geometry. Accordingly we repeated our two component fit using the values $E_b^s = -0.24$ eV and $I^s = 0.12$ found by CWB. Results for this fit are shown in figure 6(a) and table 2 (FIT 3). A Gaussian width $W = 0.30$ eV was obtained, in excellent agreement with the Gaussian broadening observed at the Cu Fermi edge. It can be seen that the residuals are extremely small and consist of statistical noise except for the low kinetic energy extreme of the spectrum where the spectral weight in the simulation underestimates the experimental intensity.

As stated above, systematics in the residuals indicate an error in the form of the fitting function. In the present case this can be attributed to the neglect in the simulation of the background arising from the inelastic scattering of photoelectrons travelling through the solid on their way to the specimen surface. A background contribution to the calculated spectrum should in principle be simulated by some physically motivated model. It remains common practice to use the 'Shirley integrated' background in which it is assumed that the background intensity at a given kinetic energy is proportional to the integrated intensity to higher kinetic energy [16]. The Shirley algorithm is equivalent to convolution by a step-like loss function with intensity independent of energy which is a rather poor approximation to real loss functions [17]. As a result the smooth step-like Shirley background cannot replicate

Table 2. LS fitting results for the Cu $2p_{3/2}$ photoelectron spectra of Cu, $Cu_{0.8}Pd_{0.2}$ and $Cu_{0.5}Pd_{0.5}$. Parameters without error bars are held fixed.

	FIT 1	FIT 2	FIT 3	FIT 4	FIT 5	FIT 6	FIT 7
Sample	Cu	Cu	Cu	$Cu_{0.5}Pd_{0.5}$	$Cu_{0.5}Pd_{0.5}$	$Cu_{0.5}Pd_{0.5}$	$Cu_{0.8}Pd_{0.2}$
E_s	—	0.27±0.03	0.24	0.27±0.05	0.25 ± 0.05	0.27 ± 0.06	0.31 ± 0.05
I_s	—	0.14 ± 0.06	0.12	0.12	0.12	0.12	0.12
Γ	0.609 ± 0.020	0.580 ± 0.013	0.594 ± 0.007	0.638 ± 0.016	0.592 ± 0.011	0.594	0.594
W	0.328 ± 0.020	0.300 ± 0.020	0.302 ± 0.020	0.3	0.366 ± 0.016	0.3	0.3
α	0.026 ± 0.005	0.034 ± 0.005	0.031 ± 0.004	0.045 ± 0.006	0.050 ± 0.005	0.050 ± 0.006	0.038 ± 0.008
λ/R	—	—	—	—	—	$(0.92 \pm 0.20) \times 10^{-3}$	$(1.20 \pm 0.20) \times 10^{-3}$
χ_r^2	1.97	0.86	0.95	1.62	1.10	1.08	0.72

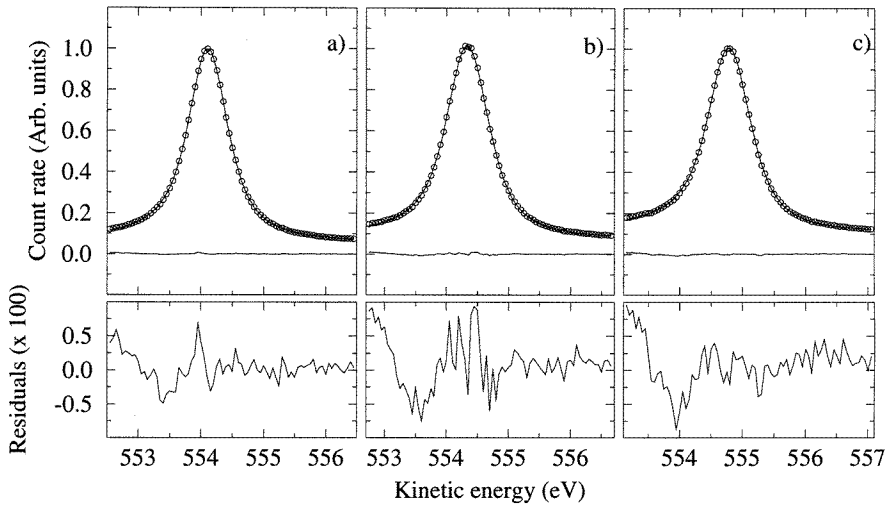

Figure 6. Experimental data (circles) and simulations (solid lines) for the Cu $2p_{3/2}$ photoelectron spectra of Cu (a), $Cu_{0.8}Pd_{0.2}$ (b) and $Cu_{0.5}Pd_{0.5}$ (c) In each case the residuals are also shown both on the same scale as the experimental data, and multiplied by 100.

plasmon satellites, for example, and in general provides a poor approximation for the real background [17].

Nonetheless Wertheim and Dicenzo [13] have suggested that for situations where the background intensity is rather low the Shirley background may prove useful. Since both the background parameter b and the asymmetry parameter α can be used to increase the spectral intensity at high binding energy these parameters can be strongly coupled [13]. We decided that the most credible procedure is to follow CWB in limiting the fitted portion of the spectrum to about 1.6 eV to the higher binding energy of the photoelectron line and neglect the background. This may lead to slight overestimates of α, but has the advantage of preserving the form of the low binding energy side of the photoelectron line where background and asymmetry effects are not present. Further justification for this approach lies in the observation of Tougard and Jorgensen [17] that the intensity of the inelastic background in the vicinity of narrow photoelectron lines can be considerably less than predicted by the Shirley background. Since we have already noted in section 4 that the backgrounds for the three specimens studied here are similar and very weak, the neglect of the background in our LS fitting is expected to give rise to small and similar errors in each case. On this basis FIT 3 represents our best fit to the experimental Cu 2p spectrum of the pure element.

5.2. $Cu_{0.5}Pd_{0.5}$

Starting with I_s, W equal to their pure Cu values given by FIT 3, we then performed LS fitting of the Cu 2p spectrum of $Cu_{0.5}Pd_{0.5}$ (FIT 4 in table 2) allowing Γ, α, E_s to vary. The values $E_s = -0.27, \alpha = 0.045, \Gamma = 0.638$ gave $\chi_r^2 = 1.62$, but strong systematics were found in the residuals. In particular the simulated line was too narrow near the centre of the peak but too broad in the tails, indicating an exaggerated Lorentzian component to the broadening. Allowing W to vary we obtained (see FIT 5 in table 2) $E_s = -0.25, \Gamma = 0.592, W = 0.366, \alpha = 0.050$ with $\chi_r^2 = 1.100$. Most importantly all

systematics were removed from the residuals, with the exception of the discrepancy at high binding energy also present for pure Cu. Though allowed to vary, E_s and Γ are essentially unchanged from their values in pure Cu. We conclude that there is an additional broadening mechanism present in the alloy and that this broadening is Gaussian in character. The results of FIT 5 correspond to an additional Gaussian broadening of 0.21 eV (added in quadrature) to that observed for pure Cu. We attribute this to disorder broadening of the electrostatic potential in the alloy.

In the light of this conclusion we performed a final fit (FIT 6) using the NNA approach of equation (19) in section 3. In this case the component spectra were DS lineshapes with Γ, W fixed at their pure Cu values. No disorder broadening of the surface component was included. In effect the only parameters varied from pure Cu are α and λ/R, the latter controlling the extent of the disorder broadening as discussed in sections 2 and 3. A value of $0.9 \times 10^{-3}e$ Å^{-1} was obtained from the fit, approximately half the expected value. The NNA fit of the $Cu_{0.5}Pd_{0.5}$ Cu 2p spectrum is shown in figure 6(c).

5.3. $Cu_{0.8}Pd_{0.2}$

An NNA fit to the Cu 2p spectrum of the $Cu_{0.8}Pd_{0.2}$ alloy was also performed. As before all parameters were fixed at their pure Cu values with the exception of α, E_s and λ/R. In this way we obtained $\alpha = 0.038$, $E_s = -0.31$, $\lambda/R = 1.2 \times 10^{-3}e$ Å^{-1} with $\chi_r^2 = 0.72$ (see FIT 7 in table 2) as shown in figure 6(b).

To summarize this section we note that the analysis of the Cu $2p_{3/2}$ spectrum of the pure metal gave good agreement with CWB. The observed core level broadening of the alloy spectra could be modelled using the NNA approach with an empirically determined value of $\lambda/R \approx 10^{-3}e$ Å^{-1}, approximately half the expected value. We found essentially no change in core hole lifetime or surface core level shifts, but a modest increase in the asymmetry parameter with Pd composition. It should be noted that since the asymmetry parameter reflects the *local* density of states at the Fermi level [11, 18] one would expect that α should vary with the local environment in a disordered alloy as well as with global composition. Since the asymmetry variation with global composition of the Cu $2p_{3/2}$ photoelectron lines in Cu_xPd_{1-x} is modest [11], the use of the same α for all components in the NNA does not introduce significant errors.

6. Discussion

Over the last decade band structure methods based on the single site coherent potential approximation (CPA) in which a single A(B) atom is embedded in an effective medium have been found to provide the best available description of the electronic structure of random substitutional binary alloys [19]. In spite of its apparent success, the standard CPA omits Madelung contributions to the total energy by construction and so yields unreliable structural properties for alloys with non-negligible charge transfer [1].

To address this shortcoming Johnson and Pinski [20] have developed the 'charge-correlated CPA' (cc-CPA). In this approach the charge on a site i is assumed to be determined solely by the number of unlike neighbours N_1, although no assumption of linearity is made. In this way the cc-CPA becomes a '$Z_1 + 1$-site' theory. By adding the electrostatic energy due to the interaction of the $Q^{i=\mathrm{A(B)}}(N_1)$ with the average Madelung potential for each given value of N_1 to the energy functional of the standard CPA, Johnson and Pinski observed [20] a dramatic improvement in the formation energies of several alloys. They also found that the self-consistently determined charges for the $Z_1 + 1$ components were linear in N_1 and

had gradient independent of composition x. Transferability appeared to hold even to the impurity limit.

Given its success, Johnson and Pinski [20] then used the cc-CPA to develop a modified single site theory. The screened-CPA (scr-CPA) is obtained by considering a single site experiencing the average Madelung potential. The scr-CPA was found to incorporate most of the Madelung energy of the cc-CPA at greatly reduced computational cost. A similar single site theory refered to as SIM-CPA has also been developed [21]. Though based on similar physics this model and the scr-CPA gave rise to Madelung energies differing by a prefactor β. The apparent discrepancy has been explained by Korzhavyi *et al* [22] who pointed out that the energy corrections in both models were approximate. By scaling the Madelung correction to reproduce thermodynamical properties of a number of alloys the optimum prefactor was found [22] to lie between 0.5 (the scr-CPA result) and 1.0 (the SIM-CPA result). Magri *et al* [2] have shown that $\beta = 0.657$ for the point charge CCM, consistent with the analysis of Korzhavyi *et al* [22]. These comparisons with first principles calculations confirm the validity and importance of point charge electrostatics and the simple charge transfer picture embodied in the CCM.

More recently the development of 'order-N' scaling methods have enabled *ab initio* calculations to be performed for disordered supercells of unprecedented size [23] and results from such calculations have been used to test the validity of both the starting assumptions and the predictions of the CCM [24, 25, 26]. The first of these comparisons was made [24] for subsitutionally disordered Cu_xZn_{1-x} alloys with a bcc lattice. While a trend of increasing charge transfer with increasing N_1 was observed, there was considerable scatter about the simple linear dependence assumed by the CCM. However for the fcc lattice the dependence of charge and nearest neighbour composition assumed in the CCM was found to be quite accurate [25, 26]. It is clear that this distinction between fcc and bcc lattices is due to the difference in ρ_2 for these structures [25]. A generalized CCM in which the charge scales linearly with both the first and second shell composition was found to give excellent agreement with *ab initio* calculations for the bcc alloys.

The success of the CCM is due to the fact that the degree of local charge neutrality implicit in the model gives a good description of metallic screening. It is instructive to consider the impurity limit. Within the CCM the central impurity site has a charge of +1 say, each first shell atom has a charge of $-1/Z_1$ and all other sites are neutral, and so the impurity is assumed to be perfectly screened by the first shell. First principles electronic structure calculations for self consistently embedded impurities [27] confirm that this is reasonable in metallic systems. A test of the internal consistency of the CCM can be made by calculating the spatial variation of the Madelung potential in the impurity limit. For the fcc lattice we find that the Madelung potential at the second shell sites is already only 3% of the Madelung potential at an impurity site. For the bcc lattice the Madelung potential at a second shell site is still 11% that of the impurity site value. Therefore the CCM has a much worse degree of internal consistency for the bcc structure.

Since the supporting evidence for the CCM for fcc systems is particularly strong we expect the CCM core XPS simulations to be quantitatively correct. However, the value $\lambda/R \approx 1.1 \pm 0.2 \times 10^{-3} e$ Å^{-1} determined empirically from the experimental data in section 5 is approximately half the value calculated by Lu *et al* [6]. There is probably a degree of uncertainty surrounding the calculated value of λ/R since this was deduced [6] from site charges obtained by a real space charge partition scheme. Any such procedure is essentially arbitrary and can give different results when applied to charge densities calculated for a given system with different *ab initio* methods [25]. Wolverton and Zunger [3] have pointed out that a more consistent definition of site charges is provided by ensuring that the resultant

electrostatic energy of the point charge model equals that obtained from first principles calculations. This uncertainty in absolute charge magnitudes may be of the order of 15% [25] and so itself does not explain the smaller than expected disorder broadening. Rather we attribute this observation to short range order in the specimens studied. Monte Carlo simulations [3] have shown that even at high temperatures there is considerable tendency for short range ordering in the CCM point charge lattice. X-ray diffraction measurements [28] confirm the propensity for short range ordering in the Cu_xPd_{1-x} alloy system. Since we have demonstrated that the core potential at a site is essentially determined by the nearest neighbour composition, short range order will quench disorder broadening rather effectively. It has also been pointed out [29] that a site dependent core hole relaxation contribution to the XPS spectra may compensate some of the variation in ground state site potential. Changes with composition in the average core hole relaxation energy at Cu sites are relatively small in the Cu_xPd_{1-x} alloy system [10]. To the authors' knowledge relaxation changes with local environment have not been studied, but could in principle increase or reduce core XPS linewidths in disordered alloys, as suggested by Matthew [29].

It is likely that high resolution core level XPS measurements can provide a useful probe of short range order. Alloy core level shifts are in principle related to the average tendency for ordering/clustering (i.e. the Warren–Cowley parameter) while the disorder broadening should furnish information about the distribution of local environments (i.e. the $P_m(N_m, c)$ function).

7. Summary

We have discussed the correlated charge model [2] in which the charge on any site is assumed to be proportional to its number of unlike neighbours N_1. We have shown that the average site potential for sites with a given N_1 is also proportional to N_1. The scatter about these averages has been characterized in terms of the contributions to the disorder in V^i due to disorder in the compositions of shells beyond the first. We have also shown that $\overline{V}^{A(B)}$, the potential averaged over all A(B) sites, is given by $\overline{Q}^{A(B)}/R$, corresponding to an effective Madelung constant of unity for all structures and all compositions. Using a realistic estimate of the model parameter λ we have shown that disorder broadening of core level XPS lines in random alloys should be observable with the resolution afforded by current XPS spectrometers. XPS data for the CuPd alloy system have demonstrated the observation of disorder broadening, but the effect was found to be significantly smaller than predicted for perfectly random alloys. We attribute this to a tendency for short range ordering implicit in the CCM. The 'nearest neighbour approximation', in which the XPS spectrum is given by the superposition of $Z_1 + 1$ components, was found to give an good description of the XPS lineshape of disordered alloys.

Acknowledgments

The contributions of G Beamson, P Unsworth and N J Brooks in obtaining experimental data are gratefully acknowledged.

References

[1] See, for example, Zunger A 1994 *Statics and Dynamics of Alloy Phase Transformations* ed P E A Turchi and A Gonis (New York: Plenum) pp 361–419

Johnson D D and Pinski F J 1994 *Metallic Alloys: Experimental and Theoretical Perspectives* ed J S Faulkner and R G Jordan (Dordrecht: Kluwer) pp 149–58
[2] Magri R, Wei S H and Zunger A 1990 *Phys. Rev.* B **42** 11388
[3] Wolverton C and Zunger A 1995 *Phys. Rev.* B **51** 6876
[4] Cole R J, Brooks N J and Weightman P 1997 *Phys. Rev. Lett.* **78** 3777
[5] Cole R J and Weightman P 1997 *J. Phys.: Condens. Matter* **9** 5609
[6] Lu Z W, Wei S H and Zunger A 1991 *Phys. Rev.* B **44** 10470
Lu Z W, Wei S H and Zunger A 1992 *Phys. Rev.* B **45** 10314
[7] There are alloy systems with greater 'ionicity' which may be expected to exhibit more dramatic disorder effects. However this tendency favours the formation of intermetallics rather than solid solutions, i.e. disordered phases may not exist. The CuPd alloy system forms substitutionally disordered alloys at all compositions and is therefore a good test case for the study of electrostatics in disordered alloys. Furthermore, Cu 2p levels excited by Al $K\alpha$ radiation give rise to photoelectron lines which are both narrow and dominated by bulk emission.
[8] Gelius U 1973 *Phys. Scr.* **9** 133
[9] In general the linear dependence of $\bar{V}$ on c may not be strictly reproduced by experimental core XPS shifts due changes in surface dipole, relaxation energy and valence configuration.
[10] Cole R J, Brooks N J and Weightman P 1998 *Phys. Rev.* B **56** 12 178
[11] Mårtensson N, Nyholm R, Calen H, Hedman J and Johansson B 1981 *Phys. Rev.* B **24** 1725
[12] Sundaram V S, de Moraes M B and Kleiman G G 1981 *J. Phys. F: Met. Phys.* **11** 1151
[13] Wertheim G K and Dicenzo S B, 1985 *J. Electron Spectrosc. Relat. Phenom.* **37** 57
[14] Citrin P H, Wertheim G K and Baer Y 1983 *Phys. Rev.* B **27** 3160
[15] Doniach S and Ŝunjić M 1970 *J. Phys. C: Solid State Phys.* **3** 285
[16] Shirley D A 1972 *Phys. Rev.* B **5** 4709
[17] Tougard S and Jorgensen B 1984 *Surf. Sci.* **143** 482
[18] Shevchik N J 1974 *Phys. Rev. Lett.* **33** 1336
[19] See, for example, Gyorffy B L, Johnson D D, Pinski F J, Nicholson D M and Stocks G M 1994 *Alloy Phase Stability* ed G M Stocks and A Gonis (New York: Plenum) p 293
[20] Johnson D D and Pinski F J 1993 *Phys. Rev.* B **48** 11553
[21] Abrikosov I A, Vekilov Yu H, Korzhavyi P A, Ruban A V and Shilkrot L E 1992 *Solid State Commun.* **83** 867
[22] Korzhavyi P A, Ruban A V, Abrikosov I A and Skriver H L 1995 *Phys. Rev.* B **51** 5773
[23] Wang Y, Stocks G M, Shelton W A, Nocholson D M C, Szotek Z and Temmermann W M 1995 *Phys. Rev. Lett.* **75** 2867
[24] Faulkner J S, Wang Y and Stocks G M 1995 *Phys. Rev.* B **52** 17106
[25] Wolverton C, Zunger A, Froyen S and Wei S H 1996 *Phys. Rev.* B **54** 7843
[26] Faulkner J S, Wang Y and Stocks G M 1997 *Phys. Rev.* B **55** 7492
[27] Zeller R 1987 *J. Phys. F: Met. Phys.* **17** 2123
[28] Saha D K, Koga K and Ohshima K 1992 *J. Phys.: Condens. Matter* **4** 10093 and references therein
[29] J A D Matthew 1997 private communication